

Electron and hole states in quantum dot quantum wells within a spherical eight-band model

E. P. Pokatilov* and V. A. Fonoberov†

Laboratory of Multilayer Structure Physics, Department of Theoretical Physics, State University of Moldova, Strada Mateevici 60, MD-2009 Chişinău, Moldova

V. M. Fomin‡ and J. T. Devreese§

Theoretische Fysica van de Vaste Stof, Departement Natuurkunde, Universiteit Antwerpen (UIA), Universiteitsplein 1, B-2610 Antwerpen, Belgium

(Received 12 April 2001; published 10 December 2001)

In order to study heterostructures composed both of materials with strongly different parameters and of materials with narrow band gaps, we have developed an approach [E. P. Pokatilov *et al.*, Phys. Rev. B **64**, 245328 (2001), preceding paper], which combines the spherical eight-band effective-mass Hamiltonian and the Burt's envelope-function representation. Using this method, electron and hole states are calculated in CdS/HgS/CdS/H₂O and CdTe/HgTe/CdTe/H₂O quantum dot quantum-well heterostructures. Radial components of the wave functions of the lowest *S* and *P* electron and hole states in typical quantum dot quantum wells (QDQW's) are presented as a function of radius. The six-band-hole components of the radial wave functions of an electron in the eight-band model have amplitudes comparable with the amplitude of the corresponding two-band-electron component. This is a consequence of the coupling between the conduction and valence bands, which gives a strong nonparabolicity of the conduction band. At the same time, the two-band-electron component of the radial wave functions of a hole in the eight-band model is small compared with the amplitudes of the corresponding six-band-hole components. It is shown that in the CdS/HgS/CdS/H₂O QDQW holes in the lowest states are strongly localized in the well region (HgS). On the contrary, electrons in this QDQW and both electron and holes in the CdTe/HgTe/CdTe/H₂O QDQW are distributed through the entire dot. The importance of the developed theory for QDQW's is proven by the fact that in contrast to our rigorous eight-band model, there appear spurious states within the commonly used symmetrized eight-band model.

DOI: 10.1103/PhysRevB.64.245329

PACS number(s): 73.21.-b, 73.40.Kp, 73.40.Lq

I. INTRODUCTION

Using colloidal growth technique it is possible to obtain both alloys and multilayer quantum dot structures. The dots are formed as free particles in a liquid medium. In principle, they may be concentrated, and redispersed in other hosts, such as organic polymers, to give highly doped materials. Recently, CdS/HgS/CdS (Refs. 1 and 2) and CdTe/HgTe/CdTe (Ref. 3) particles, termed quantum dot quantum wells (QDQW's), have been formed in water. There are three preparation stages in the synthesis of these QDQW's: (i) formation of the CdS (CdTe) core, (ii) substitution of the mercury ions for the surface cadmium ions which results in a monolayer of the HgS (HgTe) covering the core, and (iii) growing the CdS (CdTe) cap layer onto the surface of the dot. A schematic picture of typical CdS/HgS/CdS/H₂O and CdTe/HgTe/CdTe/H₂O QDQW's and their band structures are shown in Fig. 1. High-resolution transmission-electron microscopy images revealed^{2,3} that both QDQW's are not spherical, but are preferentially truncated tetrahedric particles. However, spherical shell particles are commonly considered to interpret experimental data (see Refs. 4–8).

To our best knowledge, first theoretical study of QDQW electron and hole energy spectra was made by using the parabolic approximation for the conduction and valence bands.^{4–6} However, the position of excited hole levels and the hole localization could not be explained in that model.

Therefore, it was necessary to take into account all six hole bands.⁹ Jaskolski and Bryant have applied⁷ this model to a hole in QDQW's. To obtain the electron spectrum, they have used perturbation theory for the one-band effective-mass Schrödinger equation with an energy-dependent mass correction. The present authors have also used⁸ the six-band model for a hole and the parabolic band approximation for an electron to investigate electron, hole, impurity, and exciton states

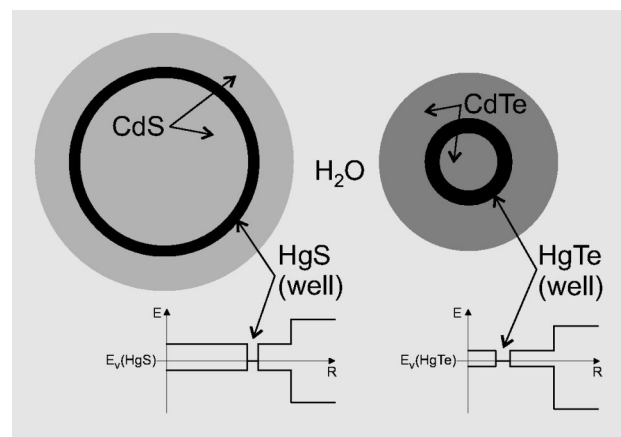


FIG. 1. A schematic picture of typical CdS/HgS/CdS (left panel) and CdTe/HgTe/CdTe (right panel) QDQW's in H₂O. Diameters of the considered QDQW's are 6.8 nm and 4.7 nm, correspondingly. The band structure of each QDQW is shown below.

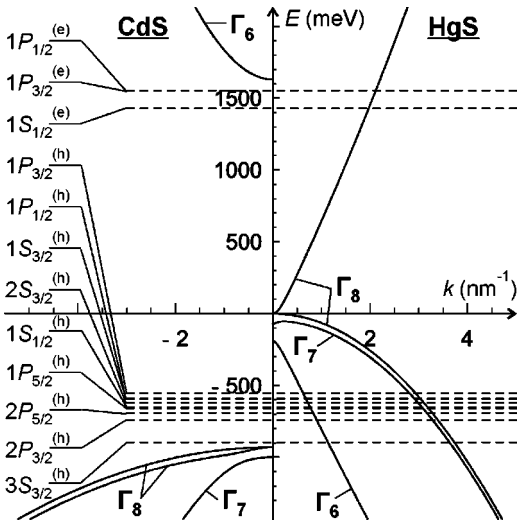


FIG. 2. The bulk eight-band structure of CdS and HgS calculated using the material parameters from Table I. Dashed horizontal lines denote the lowest S and P electron and hole energy levels in a typical CdS/HgS/CdS/H₂O QDQW (diameter=6.8 nm). The corresponding radial components of the wave functions are presented as a function of r in Fig. 4.

in QDQW's. In Refs. 7 and 8 the “symmetrized” 6×6 hole Hamiltonian has been used for the quantum dot heterostructure. In general, such a Hamiltonian can be inadequate for small nanocrystals (see Refs. 10–12).

The eight-band structure of bulk CdS and HgS is shown in Fig. 2, and the eight-band structure of bulk CdTe and HgTe is shown in Fig. 3. It is seen from these figures that the well materials HgS and HgTe are semimetals, i.e., they have a zero band gap and the conduction band with Γ_8 symmetry. As also seen from Figs. 2 and 3, the conduction band (CB) is

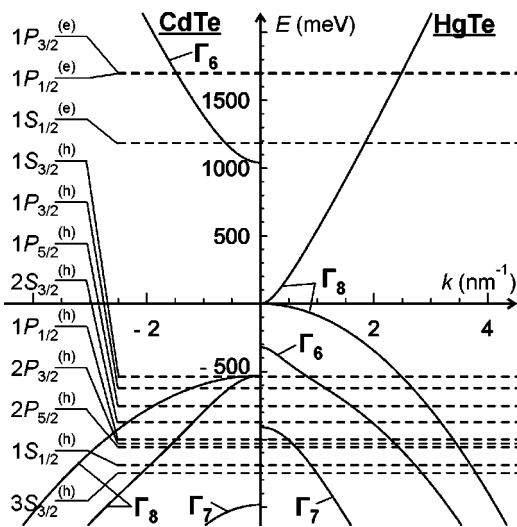


FIG. 3. The bulk eight-band structure of CdTe and HgTe calculated using the material parameters from Table I. Dashed horizontal lines denote the lowest S and P electron and hole energy levels in a typical CdTe/HgTe/CdTe/H₂O QDQW (diameter=4.7 nm). The corresponding radial components of the wave functions are presented as a function of r in Fig. 5.

parabolic only at the bottom, and even in the region of the electron ground-state energy the deviation from parabolicity is very strong. Because of the inverted band structure, the coupling between the conduction and valence bands should be included explicitly. In order to simultaneously describe the nonparabolicity of the conduction band and the influence of the conduction band on the valence bands, we consider the eight-band Pidgeon and Brown model¹³ which takes into account both the coupling of conduction and valence bands and the complex structure of the valence band (VB).

The exact electron and hole spectra are a starting point to calculate the exciton spectrum and oscillator strengths of the exciton transitions. They are required to analyze zero-phonon, one-phonon, and multiphonon lines in the photoluminescence spectra of these QDQW's, and to compare the obtained results with experiment.^{2,3,14,15} In the nonadiabatic theory¹⁶ of the phonon-assisted optical transitions in semiconductor quantum dots (QD's) the heights of the phonon peaks in the photoluminescence spectrum strongly depend on the peculiarities of the exciton spectrum. It has been proved for InSb,¹⁷ InAs,¹⁸ and InP (Ref. 19) QD's that the eight-band model is important to describe the electron and hole spectra even in spherical nanocrystals with a direct band structure. All these facts together as well as the aforementioned inadequacy of the previously used models make it desirable and useful to calculate the exact electron and hole spectra using the eight-band model.

In our previous work,²⁰ using Burt's envelope-function representation,^{21,22} we have extended the 8×8 model to include heterostructures. In the present paper we apply our rigorous eight-band model for spherical quantum dot heterostructures, namely, for QDQW's. In the next section we analyze the electron and hole states in typical QDQW's. Conclusions are given in Sec. III.

II. ELECTRON AND HOLE STATES FOR TYPICAL QDQW'S

We consider two spherical QDQW's as shown in Fig. 1. In the CdS/HgS/CdS/H₂O QDQW, the 4.4 nm in diameter CdS core is successively covered by 1 ML of HgS (0.3 nm) and 3 ML of CdS (0.9 nm). In the CdTe/HgTe/CdTe/H₂O QDQW, the 1.5 nm in diameter CdTe core is successively covered by 1 ML of HgTe (0.4 nm) and 3 ML of CdTe (1.2 nm). The eight-band energy structures of CdS/HgS and CdTe/HgTe, calculated from the bulk effective-mass parameters listed in Table I, are depicted in Figs. 2 and 3, correspondingly.

To investigate electron and hole states in QDQW's we use the eight-band effective-mass model extended to include heterostructures in Ref. 20. In spherical quantum dot heterostructures, namely, in spherical QDQW's, all effective-mass parameters entering the eight-band Hamiltonian depend only on the radial coordinate r . Therefore, electron and hole states are eigenfunctions of the total angular momentum j and its z component $m \equiv j_z$. Consequently, the electron or hole wave function can be written as a linear expansion in the eight Bloch functions $u_{J,\mu}^{c(v)}$ ($u_{J,\mu}^c$ and $u_{J,\mu}^v$ are the Bloch functions of the conduction and valence bands from Refs. 17 and 20, J

TABLE I. Eight-band bulk effective-mass parameters of the QDQW's constituent materials.

Parameters	HgS	CdS	HgTe	CdTe	H ₂ O
E_p (eV)	13.2 ^a	21.0 ^a	15.5 ^b	17.4 ^c	0 ^d
E_g (eV)	-0.190 ^a	2.56 ^a	-0.32 ^e	1.57 ^f	8.0 ^d
Δ (eV)	0.07 ^a	0.07 ^a	0.91 ^e	0.953 ^g	0 ^d
E_v (eV)	0	-0.93 ^a			-4.0 ^d
E_v (eV)			0	-0.53 ^f	-4.6 ^h
α	-1.0 ^a	-2.57 ^a	1.0 ⁱ	1.30 ^g	1 ^d
γ_1	0.35 ^a	-1.02 ^a	1.66 ^j	1.68 ^g	1 ^d
γ	-0.67 ^a	-0.75 ^a	-0.31 ^j	0.01 ^g	0 ^d

^aReference 20.^fReference 27.^bReference 24.^gReference 28.^cReference 25.^hReference 29.^dReference 7.ⁱReference 30.^eReference 26.^jReference 31.

is the Bloch function angular momentum, and $\mu \equiv J_z$ is its z component) as

$$\Psi_{j,m}(\mathbf{r}) = \sum_{\mu=-1/2}^{1/2} F_{1/2,\mu}^{c;j,m}(\mathbf{r}) u_{1/2,\mu}^c + \sum_{J=1/2}^{3/2} \sum_{\mu=-J}^J F_{J,\mu}^{v;j,m}(\mathbf{r}) u_{J,\mu}^v, \quad (1)$$

where the envelope functions $F_{J,\mu}^{c(v);j,m}(\mathbf{r})$ are

$$F_{1/2,\mu}^{c;j,m}(\mathbf{r}) = \sum_{l=j-1/2}^{j+1/2} \sum_{\lambda=-l}^l C_{1/2,\mu;l,\lambda}^{j,m} R_{1/2,l}^{c;j}(r) Y_{l,\lambda}(\theta, \phi),$$

$$F_{3/2,\mu}^{v;j,m}(\mathbf{r}) = i^{\mu-3/2} \sum_{l=|j-3/2|}^{j+3/2} \sum_{\lambda=-l}^l C_{3/2,\mu;l,\lambda}^{j,m} R_{3/2,l}^{v;j}(r) Y_{l,\lambda}(\theta, \phi), \quad (2)$$

$$F_{1/2,\mu}^{v;j,m}(\mathbf{r}) = i^{1/2-\mu} \sum_{l=j-1/2}^{j+1/2} \sum_{\lambda=-l}^l C_{1/2,\mu;l,\lambda}^{j,m} R_{1/2,l}^{v;j}(r) Y_{l,\lambda}(\theta, \phi).$$

Here, $R_{J,l}^{c(v);j}(r)$ are the radial envelope functions, $C_{J,\mu;l,\lambda}^{j,m}$ are the Clebsch-Gordan coefficients, and $Y_{l,\lambda}(\theta, \phi)$ are the spherical harmonics. In Eqs. (1) and (2), $F_{1/2,\mu}^{c;j,m}(\mathbf{r})$ are the two-band-electron components of the eight-band wave function $\Psi_{j,m}(\mathbf{r})$ (referred to as electron components in the following) and $F_{J,\mu}^{v;j,m}(\mathbf{r})$ are the six-band-hole components of the eight-band wave function $\Psi_{j,m}(\mathbf{r})$ (referred to as hole components in the following). The electron or hole eigenenergy E_j , corresponding to the wave function $\Psi_{j,m}(\mathbf{r})$, does not depend on m , because within the spherical approximation the energy spectrum is degenerate with respect to the z component of the total momentum. It is also known²⁰ that the parity p is conserved in the spherical approximation.

For electron and hole levels, obtained within the spherical eight-band model, we use a common notation: $nQ_j^{(e)}$ denotes an electron state and $nQ_j^{(h)}$ denotes a hole state, where n is the number of the level with a given symmetry and $Q = S, P, D, \dots$ is the lowest value of the momentum l in the

spherical harmonics of Eqs. (1) and (2) in front of the CB Bloch functions for an electron state and in front of the VB Bloch functions for a hole state, i.e., $Q = j - p/2$ for an electron and $Q = \min(j + p/2, |j - 3p/2|)$ for a hole.

Parameters $\xi(r)$ and $\chi(r)$ introduced in Ref. 20 are responsible for the nonsymmetrical form of the eight-band Hamiltonian. χ is explicitly defined through the effective-mass parameters of the homogeneous bulk model:

$$\chi = (5\gamma - \gamma_1 - 1)/3. \quad (3)$$

Following Refs. 20 and 23 we take for ξ ,

$$\xi = v. \quad (4)$$

Using our rigorous eight-band model and the aforementioned set of parameters, the lowest S and P electron and hole states in both QDQW's are analyzed. The $1S_{1/2}^{(e)}$, $1P_{3/2}^{(e)}$, and $1P_{1/2}^{(e)}$ electron and $1P_{3/2}^{(h)}$, $1P_{1/2}^{(h)}$, $1S_{3/2}^{(h)}$, $2S_{3/2}^{(h)}$, $1S_{1/2}^{(h)}$, $1P_{5/2}^{(h)}$, $2P_{5/2}^{(h)}$, $2P_{3/2}^{(h)}$, and $3S_{3/2}^{(h)}$ hole energy levels are presented and the corresponding radial wave functions are plotted as a function of r in Figs. 4 and 5, respectively, for CdS/HgS/CdS/H₂O and CdTe/HgTe/CdTe/H₂O QDQW's. In these figures, the following denotations:²⁰

$$R_{1/2,j-1/2}^{c;j} = R_{c,j}^+, \quad R_{1/2,j+1/2}^{c;j} = -R_{c,j}^-, \quad (5)$$

$$R_{3/2,j+1/2}^{v;j} = R_{h1,j}^+, \quad R_{3/2,j-1/2}^{v;j} = R_{h1,j}^-,$$

$$R_{3/2,j-3/2}^{v;j} = -R_{h2,j}^+, \quad R_{3/2,j+3/2}^{v;j} = -R_{h2,j}^-,$$

$$R_{1/2,j+1/2}^{v;j} = R_{s,j}^+, \quad R_{1/2,j-1/2}^{v;j} = R_{s,j}^-$$

are used for the radial components $R_c(r)$ (solid curves), $R_{h1}(r)$ (dashed curves), $R_{h2}(r)$ (dotted curves), and $R_s(r)$ (dash-dotted curves). For all eigenstates, the contribution to the normalization integral $\int_0^\infty r^2 dr [R_c^2(r) + R_{h1}^2(r) + R_{h2}^2(r) + R_s^2(r)] = 1$ from each particular radial component is indicated in percent. The vertical lines in Figs. 4 and 5 represent the spherical borders between the different materials.

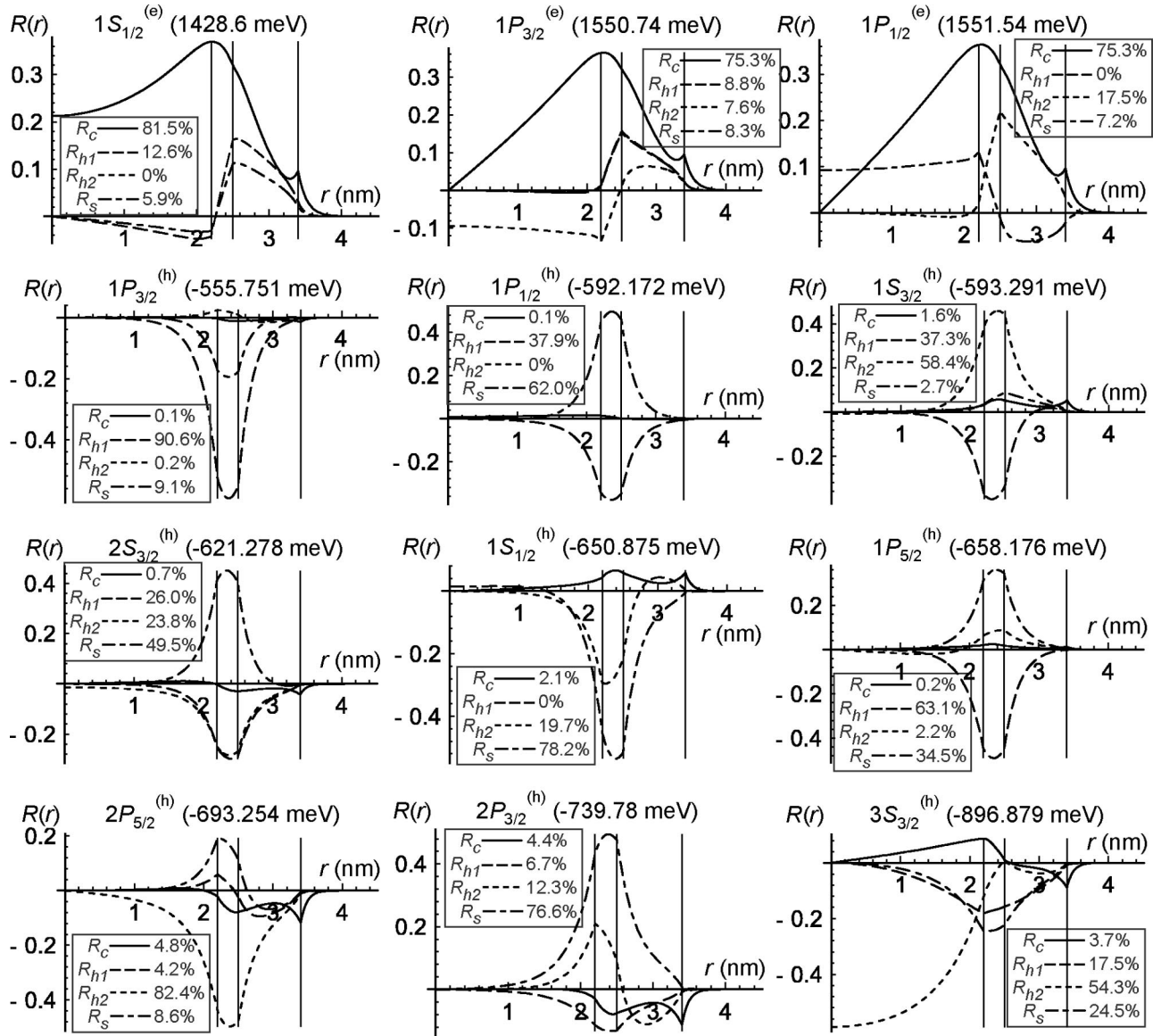


FIG. 4. The lowest S and P electron and hole energy levels and corresponding radial components of the wave functions for a typical CdS/HgS/CdS/H₂O QDQW. The contribution to the normalization integral from each radial component is indicated. Vertical lines represent the spherical boundaries which separate the CdS core, the HgS monolayer, the CdS cap layer, and the surrounding medium.

The function $R_c(r)$ is further called the electron radial component of the wave function because in Eqs. (1) and (2) it is written in front of the CB Bloch functions. The functions $R_{h1}(r)$, $R_{h2}(r)$, and $R_s(r)$ are further called the hole radial components of the wave function because in Eqs. (1) and (2) they are written in front of the VB Bloch functions. If the coupling of the conduction and valence bands is not considered, the electron wave function is described by the first term in Eq. (1) (i.e., by the electron radial component), and the hole wave function is described by the second term in Eq. (1) (i.e., by the hole radial components). The inclusion of the coupling between the conduction and valence bands (which is realized in the eight-band model) results in the fact that the electron wave function includes the six-band-hole components (HE), in addition to the two-band-electron component (EE), and the hole wave function includes the two-band-

electron component (EH), in addition to the six-band-hole components (HH).

The main radial component for the electron wave functions is the EE. As seen from Figs. 4 and 5, the amplitude of the HE is about 1/2 of the EE. It is also seen that about 20% of the contribution into the normalization integral comes from the HE. Such a big contribution from the hole components is because of the strong nonparabolicity of the conduction band in the well materials (see Figs. 2 and 3). The spin-orbit splitting of the electron levels, when going from the one-band model to the eight-band model, is very small. For example, the level $1P^{(e)}$ splits into levels $1P_{1/2}^{(e)}$ and $1P_{3/2}^{(e)}$ with the distance between them only 0.8 meV for the CdS/HgS/CdS/H₂O QDQW and 3.6 meV for the CdTe/HgTe/CdTe/H₂O QDQW. It should be noted that this splitting occurs in such a way that the lowest level in the

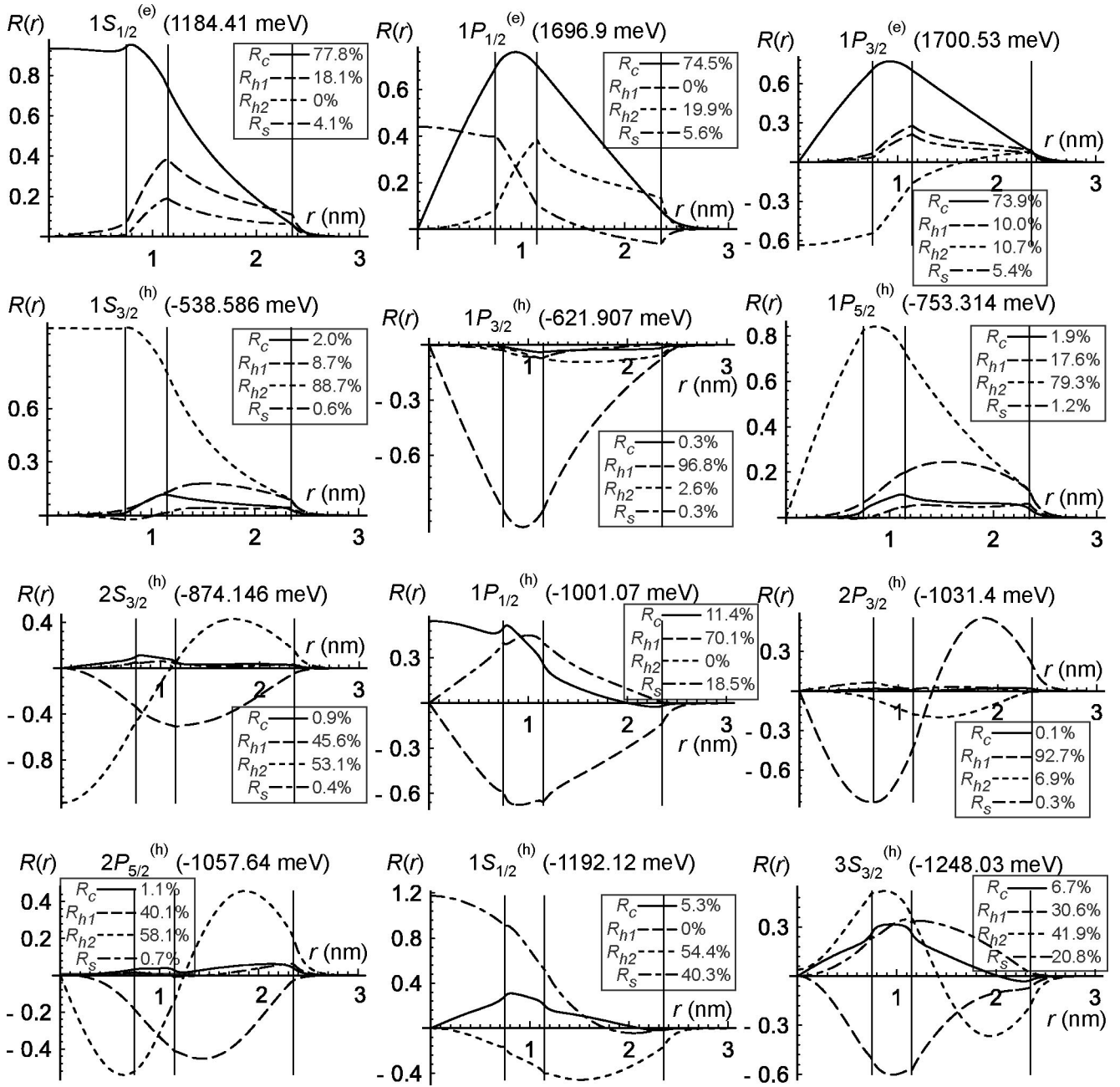


FIG. 5. The lowest S and P electron and hole energy levels and corresponding radial components of the wave functions for a typical CdTe/HgTe/CdTe/H₂O QDQW. The contribution to the normalization integral from each radial component is indicated. Vertical lines represent the spherical boundaries which separate the CdTe core, the HgTe monolayer, the CdTe cap layer, and the surrounding medium.

former QDQW is $1P_{3/2}^{(e)}$ and the lowest level in the latter QDQW is $1P_{1/2}^{(e)}$. The electron ground-state energy is not split and it is $1S_{1/2}^{(e)}$ for both QDQW's.

Three HH are the main components in the hole wave functions. The amplitude of the EH here is about 1/10 of the amplitudes of the HH, and this component gives a very small contribution into the normalization integral. Comparing with the six-band model, no additional splitting of the hole levels occurs in the eight-band model. Although the hole ground state remains $1P_{3/2}^{(h)}$ in the CdS/HgS/CdS/H₂O QDQW, the position of the hole levels changes within this model (com-

pare with Ref. 7). The hole ground energy in the CdTe/HgTe/CdTe/H₂O QDQW is $1S_{3/2}^{(h)}$.

One can see that the number of electron levels in an arbitrary energy interval is less than the number of hole levels in the same interval. This is connected with the complex structure of the valence band and with the fact that the hole effective masses are larger than the electron effective mass. The positions of an electron and a hole differ significantly in the CdS/HgS/CdS/H₂O QDQW. While the electron is distributed through the entire dot, the hole is almost completely localized in the HgS layer. It is worth pointing out that in this QDQW, the electron quantization energy is several times

larger than the hole quantization energy. Therefore, while the holes do not practically penetrate into the exterior medium, the probability of the electron presence in H_2O is about 5%. In the $\text{CdTe}/\text{HgTe}/\text{CdTe}/\text{H}_2\text{O}$ QDQW, the electron and hole behave similarly: both charge carriers are distributed through the entire dot and the probability of their presence in H_2O is about 5%. This difference between the considered QDQW's can be explained by the fact that the lowest-energy levels in the $\text{CdS}/\text{HgS}/\text{CdS}/\text{H}_2\text{O}$ QDQW lie inside the HgS well, while the lowest-energy levels in the $\text{CdTe}/\text{HgTe}/\text{CdTe}/\text{H}_2\text{O}$ QDQW lie outside the HgTe well (see Figs. 2 and 3).

Finally, taking the $\text{CdS}/\text{HgS}/\text{CdS}/\text{H}_2\text{O}$ QDQW as an example, we examine, first, what error occurs if one uses the symmetrized eight-band Hamiltonian to find electron and hole states, and, second, how electron and hole states can change if one supposes that HgS is not a semimetal with $E_g = -190$ meV, but a narrow-gap semiconductor with $E_g = 200$ meV.

The use of the symmetrized eight-band Hamiltonian leads to the following changes in the electron and hole spectra as compared to the spectra obtained within our rigorous approach. (i) For every value of total angular momentum and parity, there appears one spurious electron level with energy about 1080 meV, 1100 meV, 1120 meV, . . . for the S, P, D, \dots electron states, respectively. These electron states are spurious, because about 99% of the electron density is concentrated in a very narrow region (less than 0.5 nm wide) near the boundary between the QDQW and water. (ii) At the same time, the energy of the lowest genuine electron levels increases by 66 meV, 43 meV, 11 meV, . . . for the S, P, D, \dots electron states, respectively. Since all other electron states must be orthogonal to the lowest — spurious — state, a considerable part of the low-lying electron states possesses a high probability (about 1/2) that the electron is in water. (iii) The energy of hole states changes only slightly (by ± 5 meV). The density of the lowest hole states is also slightly modified.

The increase of the value $E_g(\text{HgS})$ from -190 meV to 200 meV, while all other parameters are kept unchanged, results in the following. (i) The energy of all the lowest electron levels increases by about 80 meV. This fact leads to a decrease of the electron density in the HgS well and to a corresponding increase of the electron density in the CdS

layers. (ii) The energy of hole levels changes weakly (by less than 1 meV), and the distribution of the hole density is practically unchanged.

III. CONCLUSIONS

A spherical QDQW structure is considered within the eight-band model. This approach generalizes the one-band and the six-band models, which have been used for QDQW's so far, and exactly takes into account the nonparabolicity of the electron dispersion law. Electron and hole energy spectra and the corresponding wave functions for typical QDQW's have been examined. While in the $\text{CdS}/\text{HgS}/\text{CdS}/\text{H}_2\text{O}$ QDQW (recently considered in the framework of the six-band model⁷) holes in the lowest states are strongly localized in the well region, in the $\text{CdTe}/\text{HgTe}/\text{CdTe}/\text{H}_2\text{O}$ QDQW holes are shown to be distributed through the entire dot. At the same time, electrons in both types of QDQW's are not localized in the quantum well.

The lowest optically active electron-hole pair state in both QDQW's is $1S_{1/2}^{(e)}-1S_{3/2}^{(h)}$. The energy of this state is 2.022 eV for the $\text{CdS}/\text{HgS}/\text{CdS}/\text{H}_2\text{O}$ QDQW and 1.723 eV for the $\text{CdTe}/\text{HgTe}/\text{CdTe}/\text{H}_2\text{O}$ QDQW. The inclusion of the exciton effect reduces each of these energies by about 100 meV and makes them close to the experimental values given in Refs. 2 and 3 (the analysis of this effect is in progress). The aforementioned conclusions about the properties of the electron and hole spectra are a consequence of the 1 ML thickness of the HgS (HgTe) well and of the semimetal character of the well material. We have made certain that the symmetrized eight-band model is not capable of describing electronic states in QDQW's composed of materials with very dissimilar band parameters. It has been also shown that the obtained results do not depend critically on the actual value of the well band gap. In summary, we have demonstrated that the developed model is an effective tool to analyze quantum dot heterostructures, which include thin well layers and also narrow-band-gap materials.

ACKNOWLEDGMENTS

This work has been supported by the GOA BOF UA 2000, IUAP, FWO-V Project Nos. G.0287.95 and G.0274.01N, the W.O.G. WO.025.99N (Belgium), and CRDF Award No. MP2-2281 (Moldova).

*Electronic address: pokatilov@add.moldova.su

†Electronic address: URL: <http://www.geocities.com/fonobero/>

‡Permanent address: Laboratory of Multilayer Structure Physics, Department of Theoretical Physics, State University of Moldova, Strada Mateevici 60, MD-2009 Chişinău, Moldova. Electronic address: fomin@uia.ua.ac.be

§Also at Universiteit Antwerpen (RUCA), Groenenborgerlaan 171, B-2020 Antwerpen, Belgium and Technische Universiteit Eindhoven, P. O. Box 513, 5600 MB Eindhoven, The Netherlands. Electronic address: devreese@uia.ua.ac.be

¹A. Mews, A. Eychmüller, M. Giersig, D. Schooss, and H. Weller, *J. Phys. Chem.* **98**, 934 (1994).

²A. Mews, A.V. Kadavanich, U. Banin, and A.P. Alivisatos, *Phys. Rev. B* **53**, R13 242 (1996).

³S.V. Kershaw, M. Burt, M. Harrison, A. Rogach, H. Weller, and A. Eychmüller, *Appl. Phys. Lett.* **75**, 1694 (1999).

⁴D. Schooss, A. Mews, A. Eychmüller, and H. Weller, *Phys. Rev. B* **49**, 17 072 (1994).

⁵M. Tkach, V. Holovatsky, O. Voitsekhivska, and M. Mikhaliova, *Phys. Status Solidi B* **203**, 373 (1997).

⁶K. Chang and J.-B. Xia, *Phys. Rev. B* **57**, 9780 (1998).

⁷W. Jaskolski and G. Bryant, *Phys. Rev. B* **57**, R4237 (1998).

⁸E.P. Pokatilov, V.A. Fonoberov, V.M. Fomin, S.N. Klimin, and J.T. Devreese, *Bull. Am. Phys. Soc.* **45**, 988 (2000).

⁹G.B. Grigoryan, E. Kazaryan, Al. L. Efros, and T.V. Yazeva, *Fiz. Tverd. Tela (Leningrad)* **32**, 1772 (1990) [*Sov. Phys. Solid State* **32**, 1031 (1990)].

¹⁰B.A. Foreman, *Phys. Rev. B* **48**, 4964 (1993).

- ¹¹A.T. Meney, B. Gonul, and E.P. O'Reilly, *Phys. Rev. B* **50**, 10 893 (1994).
- ¹²S. De Franceschi, J.M. Jancu, and F. Beltram, *Phys. Rev. B* **59**, 9691 (1999).
- ¹³C.R. Pidgeon and R.N. Brown, *Phys. Rev.* **146**, 575 (1966).
- ¹⁴F. Koberling, A. Mews, and T. Basche, *Phys. Rev. B* **60**, 1921 (1999).
- ¹⁵A.T. Yeh, G. Cerullo, U. Banin, A. Mews, A.P. Alivisatos, and Ch.V. Shank, *Phys. Rev. B* **59**, 4973 (1999).
- ¹⁶V.M. Fomin, V.N. Gladilin, J.T. Devreese, E.P. Pokatilov, S.N. Balaban, and S.N. Klimin, *Phys. Rev. B* **57**, 2415 (1998).
- ¹⁷Al. L. Efros and M. Rosen, *Phys. Rev. B* **58**, 7120 (1998).
- ¹⁸U. Banin, J.C. Lee, A.A. Guzelian, A.V. Kadavanich, A.P. Alivisatos, W. Jaskolski, G. Bryant, Al. L. Efros, and M. Rosen, *J. Chem. Phys.* **109**, 2306 (1998).
- ¹⁹P.C. Sercel, Al. L. Efros, and M. Rosen, *Phys. Rev. Lett.* **83**, 2394 (1999).
- ²⁰E.P. Pokatilov, V.A. Fonoberov, V.M. Fomin, and J.T. Devreese, *Phys. Rev. B* **64**, 245328 (2001), preceding paper.
- ²¹M.G. Burt, *J. Phys.: Condens. Matter* **4**, 6651 (1992).
- ²²M.G. Burt, *J. Phys.: Condens. Matter* **11**, 53 (1999).
- ²³B.A. Foreman, *Phys. Rev. B* **56**, R12 748 (1997).
- ²⁴Y. Guldner, C. Rigaux, M. Grynberg, and A. Mycielski, *Phys. Rev. B* **8**, 3875 (1973).
- ²⁵M.L. Redigolo, W.A. Arellano, L.C. Barbosa, C.H. Brito Cruz, C.L. Cesar, and A.M. de Paula, *Semicond. Sci. Technol.* **14**, 58 (1999).
- ²⁶N. Orłowski, J. Augustin, Z. Golacki, C. Janowitz, and R. Manzke, *Phys. Rev. B* **61**, R5058 (2000).
- ²⁷D. Eich, K. Ortner, U. Groh, Z.H. Chen, C.R. Becker, G. Landwehr, R. Fink, and E. Umbach, *Phys. Status Solidi A* **173**, 261 (1999).
- ²⁸G.N. Aliev, O.S. Coschug, A.I. Nesvizski, R.P. Seisyan, and T.V. Yazeva, *Fiz. Tverd. Tela (Leningrad)* **35**, 1514 (1993) [*Sov. Phys. Solid State* **35**, 764 (1993)].
- ²⁹A.H. Nethercot, *Phys. Rev. Lett.* **33**, 1088 (1974).
- ³⁰M. von Truchsess, A. Pfeuffer-Jeschke, C.R. Becker, G. Landwehr, and E. Batke, *Phys. Rev. B* **61**, 1666 (2000).
- ³¹F.M. Gashimzade, A.M. Babaev, and M.A. Bagirov, *J. Phys.: Condens. Matter* **12**, 7923 (2000).